Accepted version of: F. Pieterse and W. P. du Plessis, “Implementation and Testing of a Retrodirective Cross-Eye Jammer,” *IEEE Transactions on Aerospace and Electronic Systems*, vol. 58, no. 5, pp. 4486–4494, Oct. 2022. Published version is available online at: http://ieeexplore.ieee.org/document/9745819

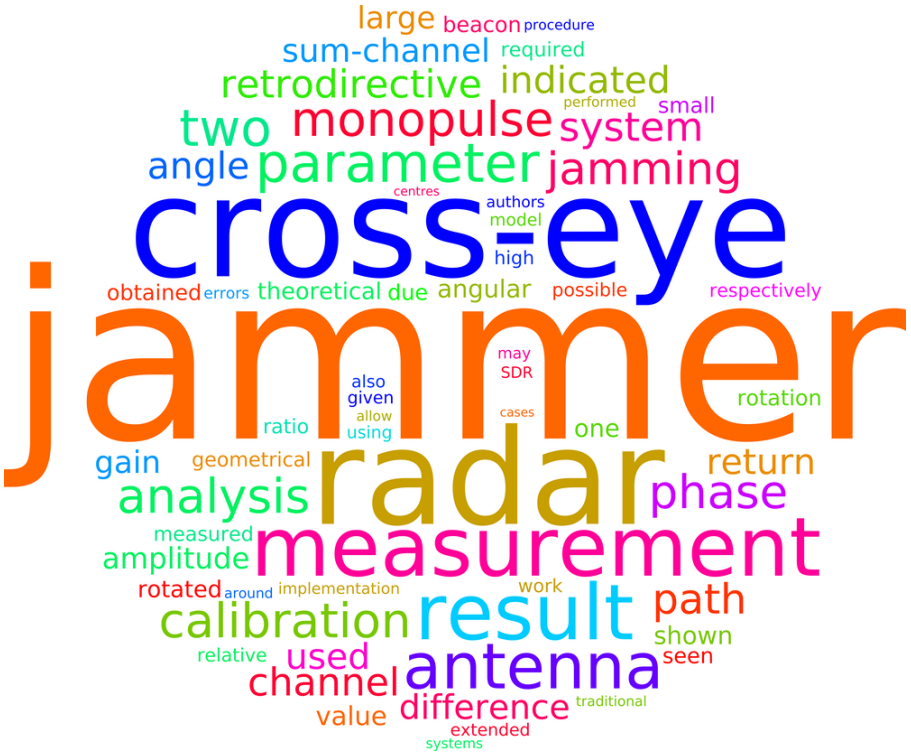

ABBREVIATIONS

CSIR	Council for Scientific and Industrial Research
DRFM	digital radio-frequency memory
EA	electronic attack
EM	electromagnetic
EW	electronic warfare
JSR	jammer-to-signal ratio
LFM	linear frequency modulation
SDR	software-defined radio
SNR	signal-to-noise ratio
SQP	sequential quadratic programming
USB	Universal Serial Bus

Implementation and Testing of a Retrodirective Cross-Eye Jammer

F. PIETERSE, *Member, IEEE* and
W. P. DU PLESSIS, *Senior Member, IEEE*

***Abstract*—One of the few electronic attack (EA) techniques that can deceive radars in angle is cross-eye jamming, which mimics the naturally-occurring phenomenon glint. The extreme tolerance requirements of cross-eye jamming mean that a retrodirective implementation is required, but published measurements of cross-eye jamming either ignore the retrodirective implementation or only simulate it. The implementation of a retrodirective cross-eye jammer and its testing against a monopulse radar are described. A procedure for calibrating the jammer is outlined and is shown to be effective by achieving large angular errors. The measured results agree well with the extended analysis of cross-eye jamming and confirm that the implemented jammer is retrodirective. Specifically, the ability of a cross-eye jammer to generate an indicated angle that never becomes zero, thereby potentially breaking a tracking lock, is confirmed.**

***Index Terms*—Cross-eye jamming, monopulse, electronic warfare (EW), electronic attack (EA), radar countermeasures, and angular deception.**

Manuscript received 20 November 2021; revised 28 February 2022; accepted 21 March 2022. The authors acknowledge the Council for Scientific and Industrial Research (CSIR) for allowing the use of their anechoic chamber.

F. Pieterse (e-mail: fpieterse@ieee.org) and W. P. du Plessis (e-mail: wduplessis@ieee.org) are with the Department of Electrical, Electronic and Computer Engineering, University of Pretoria, Pretoria, 0002, South Africa.

I. INTRODUCTION

Cross-eye jamming is an electronic attack (EA) method that can potentially be used to deceive radars in angle [1]–[6]. Cross-eye jamming artificially recreates the worst case of glint, which is a naturally-occurring phenomenon that creates angular errors in all radars due to the interaction of multiple scatterers on complex target platforms [7].

Cross-eye jamming analyses are provided in the literature [1], [5], [6], [8], and most are variations of the phase-front [9] and linear-fit [10] analyses, which are adapted from analyses of glint. However, these analyses are limited by assuming either that the radar antenna is infinitesimally small and thus responds to the fields at a point or that monopulse antenna patterns are linear, both leading to significant errors when considering cross-eye jamming [5], [6]. More importantly, these analyses omit retrodirectivity, which appears to be the only practical approach to implementing an operational cross-eye jammer [2], [4], [5].

The limitations of these analyses went unnoticed until a new analysis that made fewer assumptions was published [5], [6]. This extended analysis is based on the assumption that the radar and jammer are operating in their far- and near-field regions, respectively, as required for cross-eye jamming [8]. Additionally, the assumed monopulse antenna meant that the non-linear patterns of real monopulse antennas were accounted for in a manner that is representative of all monopulse radars [5], [11].

It can be argued that the limitations in the traditional cross-eye jamming analyses went unnoticed due to the lack of controlled measurements, and the lack of measurements was likely due to the lack of the technologies necessary to implement a retrodirective cross-eye jammer. For example, it has been argued that digital systems are necessary to implement a cross-eye jammer [12]. This is due to the extreme tolerance requirements [5], [13] and the high jammer-to-signal ratio (JSR) required [14]–[16] which both mean that high-performance systems such as digital radio-frequency memories (DRFMs) are required.

The best-known cross-eye jamming measurements are probably those presented by Neri and show cross-eye jammers operating on aircraft and ships [17], but very little information is provided. Falk alludes to measurements performed at sea without supplying any further information [12]. Similarly, du Plessis describes experiments

conducted, but again, no details are given [18]. Secret programmes doubtless also exist, but the authors are not aware of publications resulting from such work. While such measurements are useful in demonstrating that cross-eye jamming can create significant angular errors in realistic scenarios of varying degrees of complexity, they are not performed under the controlled conditions required for scientific experiments.

Some efforts to overcome this difficulty have been published, but these measurements are all limited in some way. The main approach is to perform measurements where the jammer system only transmits signals (i.e. the jammer has no receivers) and the radar system only receives signals (i.e. the radar has no transmitter) [19], [20]. Such measurements confirm the validity of traditional cross-eye jamming analyses because the underlying assumptions are the same. However, these measurements ignore the retrodirective implementation and do not accurately simulate either the radar or the jammer. Measurements that simulate a retrodirective cross-eye jammer by activating one of the paths through the jammer at a time and later combining these measurements overcome most of these concerns [5], [21]. However, these measurements only simulate a retrodirective cross-eye jammer by combining measurements, so it is possible that important factors are not accounted for.

Recently, initial results of tests of a retrodirective cross-eye jammer against a monopulse radar were described [22]. The procedure used and the results obtained are expanded on in this work. Specifically, a compensation procedure to allow comparisons to theoretical analyses is provided, and the results are shown to validate the extended analysis. This includes confirming that a retrodirective cross-eye jammer can induce an indicated angle that never becomes zero in a threat radar, thereby raising the possibility of breaking a tracking lock. This result is important as traditional analyses of cross-eye jamming reject this possibility. Additionally, a procedure to calibrate a cross-eye jammer is outlined as this was a prerequisite to the measurements. Finally, the use of low-cost software-defined radio (SDR) hardware shows that the stringent tolerance requirements of cross-eye jammers can be achieved more easily than may have been expected.

Section II provides a brief overview of monopulse radar, cross-eye jamming, and published analyses thereof. The implementation of both a monopulse radar and a cross-eye jammer are presented in Section III, including the procedure used to calibrate the jammer. Section IV describes the measurement configuration and procedures used to extract the system parameters and compensate for non-ideal aspects of the measurements to allow comparisons to theoretical results. The results obtained are presented and discussed in Section V. Finally, the work is concluded by a summary in Section VI.

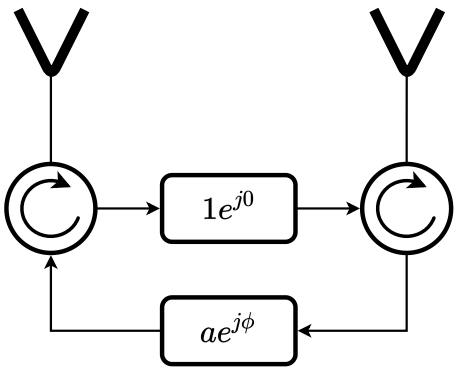

Fig. 1. Retrodirective paths of the cross-eye jammer [2].

II. Theoretical Background

A. Monopulse Radar

Phase-comparison monopulse radar implicitly uses the phase difference between the radar return at two spaced antennas to determine the monopulse ratio, which is a metric that is related to the angle towards the target [3]. This is done in the one-dimensional case by dividing the difference of the two returns by the sum of the two returns. The division ensures that the monopulse ratio is independent of signal strength, and makes the system more robust [3]. Lastly, the imaginary part of the results is kept. The monopulse ratio can be expressed as [3]

$$M = \mathcal{I}m\left\{\frac{D}{S}\right\} \tag{1}$$

$$= \tan\left[\beta\frac{d_r}{2}\sin(\theta)\right], \tag{2}$$

where D and S are the difference- and sum-channel returns, respectively. The spacing between the radar elements is given by d_r, and the angle to the target is given by θ. Lastly, the phase-propagation constant of electromagnetic (EM) radiation is given by β.

B. Cross-eye Jamming

Cross-eye jamming induces large angular errors by creating two widely-spaced returns with approximately equal amplitudes and a phase difference of close to 180° [1]–[6]. This causes the radar return from the scatterers to cancel when forming the sum-channel return, and to add when forming the difference channel return, thereby leading to a large indicated angle.

The need to maintain a phase difference of very close to 180° means that a cross-eye jammer will be

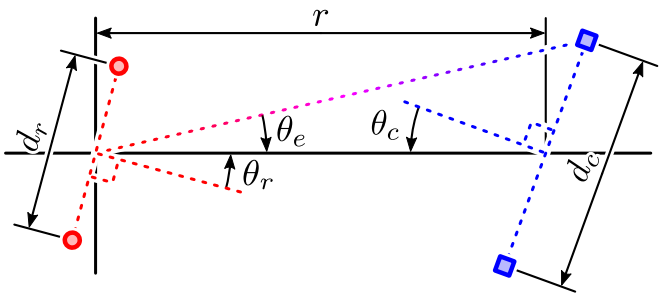

Fig. 2. The geometry of an engagement between a cross-eye jammer and radar. The radar and jammer antennas are indicated by circles and squares, respectively [6].

extremely sensitive to rotation, unless retrodirectivity is exploited [2], [4], [5]. Retrodirectivity arises when a signal incident on a repeater is retransmitted back in the same direction regardless of the rotation of the repeater. One antenna pair of a Van-Atta retrodirective array is shown in Fig. 1 [23], and setting $a \to 1$ and $\phi \to \pi$ will lead to a retrodirective cross-eye jammer.

It should also be noted that although cross-eye jamming can potentially induce enormous angular errors in radars, it is very sensitive to the values of the relative amplitude, a, and phase difference, ϕ, between the paths [5], [13]. If these parameters deviate too much from the ideal, the retrodirective property of the cross-eye jammer could potentially turn the system into a beacon, endangering the platform under protection [5], [13].

C. Traditional Analysis of Cross-eye Jamming

One approach to the traditional analysis is undertaken by assuming linear fits to the sum- and difference-channel antenna patterns [1], [5], [24]. In reality, this approximation is only valid around the boresight direction and becomes inaccurate as the radar is rotated. Using this approximation, the indicated angle of the monopulse radar can be written as [3]

$$\theta_i \approx k_m M, \tag{3}$$

where θ_i is the indicated angle, k_m is a constant, and M is the monopulse ratio.

The traditional analysis of cross-eye jamming is then obtained by considering the return from two point sources, where one point source has an amplitude factor, a, and phase difference, ϕ, relative to the other source. This resultant function for the indicated angle, θ_i, can then be expressed as [1], [24]

$$\theta_i \approx \theta_r + \theta_e G_C, \tag{4}$$

where θ_r is the rotation of the radar, θ_e is half the angular separation between the sources as viewed by the radar,

$$\theta_e \approx \frac{d_c}{2r}\cos\left(\theta_c\right), \tag{5}$$

where θ_c is the jammer rotation, and G_C is metric called the cross-eye gain, given by [4]

$$G_C = \frac{1-a^2}{1+a^2+2a\cos(\phi)}. \tag{6}$$

The angles θ_r, θ_c, and θ_e are illustrated in Fig. 2, where the geometry of the engagement between a monopulse radar and cross-eye jammer is shown.

D. Extended Analysis of Cross-eye Jamming

The extended analysis considers the geometry of a cross-eye jammer in the presence of a phase-comparison monopulse radar shown in Fig. 2 [5], [6]. The the two retrodirective jammer paths are accounted for by this analysis, and effects of the non-linear monopulse ratio are taken into account.

The derived monopulse ratio is given by [5], [6]

$$M = \frac{\sin\left(2k\right) + \sin\left(2k_c\right) G_C}{\cos\left(2k\right) + \cos\left(2k_c\right)}, \tag{7}$$

where

$$k = \beta\frac{d_r}{2}\sin\left(\theta_r\right)\cos\left(\theta_e\right) \tag{8}$$

$$k_c = \beta\frac{d_r}{2}\sin\left(\theta_e\right)\cos\left(\theta_r\right). \tag{9}$$

The result of the extended analysis in (7) led to a number of new conclusions about cross-eye jamming that were somewhat controversial. One of these new conclusions was that a cross-eye jammer can create a situation where the indicated angle never becomes zero, thereby breaking a monopulse-radar lock, something that was previously considered impossible (e.g. [1], [2]).

III. Methodology

A basic one-dimensional phase-comparison monopulse radar was implemented and used as a platform for the development, calibration, and testing of a retrodirective cross-eye jammer in an anechoic environment. A one-dimensional system is sufficient as cross-eye jammers only induce angular errors in one dimension [5].

A. Hardware Configuration

Both the radar and the jammer were implemented using Nuand bladeRF 2.0 SDRs. The choice of this device was based on the fact that the SDR has two inputs and two outputs, and operates over a wide range

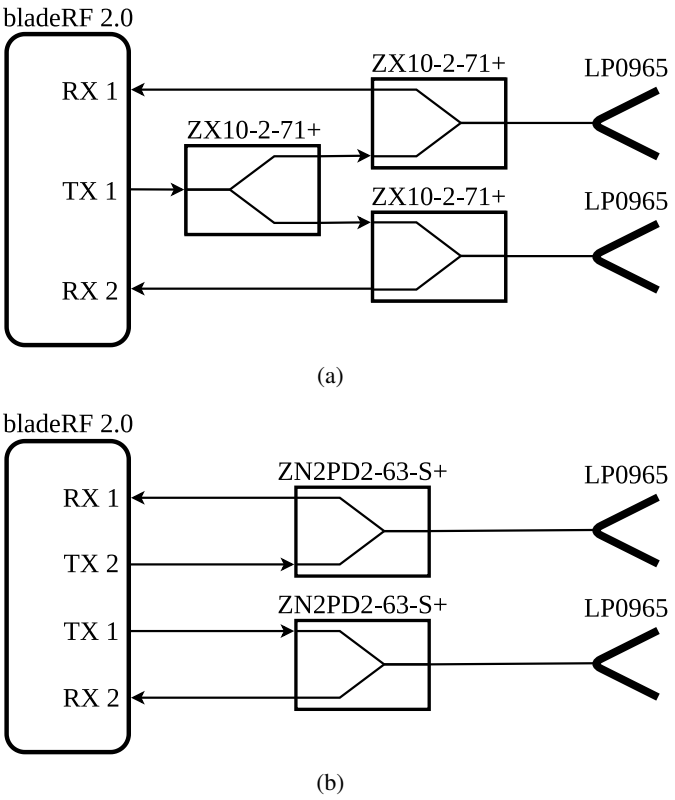

Fig. 3. Connections between the (a) radar and (b) jammer SDRs and their antennas using power dividers [22].

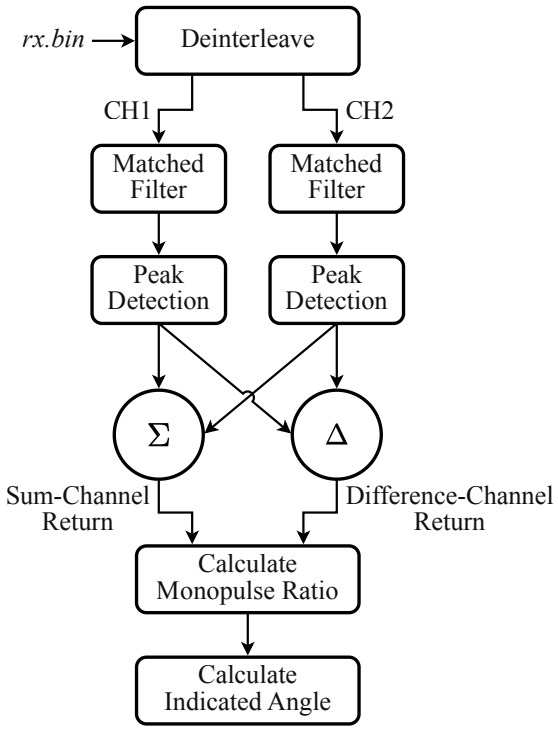

Fig. 4. Flow diagram of the radar processing.

of frequencies (47 MHz to 6 GHz). In addition, the two receive channels and two transmit channels of the device are synchronized, and coherency is important for both the reception in monopulse radar and the retrodirective operation of a cross-eye jammer [3], [5]. The radar and jammer bladeRF 2.0 SDRs were connected to different computers that were completely independent of one another.

In each case, the SDR was connected to two Ettus LP0965 log-periodic antennas using power dividers. The antennas were selected due to their wide bandwidth. For the radar, the SDR was connected to the antennas using three Mini-Circuits ZX10-2-71+ power dividers as illustrated in Fig. 3(a). For the jammer, two Mini-Circuits ZN2PD2-63-S+ power dividers were used due to their isolation of over 15 dB between port 1 and port 2, which helped to reduce the feedback suppression required from the jammer system. The configuration of the jammer hardware can be seen in Fig. 3(b). Even though the use of power dividers resulted in losses, the close proximity of the radar and the jammer due to the limited space in the anechoic chamber made these losses insignificant.

The minimum specified frequency of the Mini-Circuits ZX10-2-71+ power dividers is 2.95 GHz, so a carrier frequency of 3 GHz was used. A higher frequency would have meant that the radar was not in the near field of the cross-eye jammer.

B. Monopulse Radar Implementation

The radar was implemented by transmitting a single linear frequency modulation (LFM) pulse with a bandwidth of 0.6 MHz and processing the return received in each of the two channels. The processing is illustrated in the flow diagram in Fig. 4.

The first step was the deinterleaving of the samples that were received by the SDR to yield two complex arrays, each representing one of the channels. Pulse compression was then applied to the data, after which peak detection was performed to isolate the radar return for each channel. The radar returns were then added together and subtracted from one another to form the sum- and difference channel returns, respectively. The latter was divided by the former, and the imaginary part was kept, to form the monopulse ratio of the radar as shown in (1). Lastly, the indicated angle was determined by using the monopulse ratio to solve for θ in (2).

The beamwidth of the radar antennas was not measured as the relevant facilities were not available. Simulations of the radar antenna in Feko 2021.1 indicated that the sum-channel beamwidth was approximately 20°.

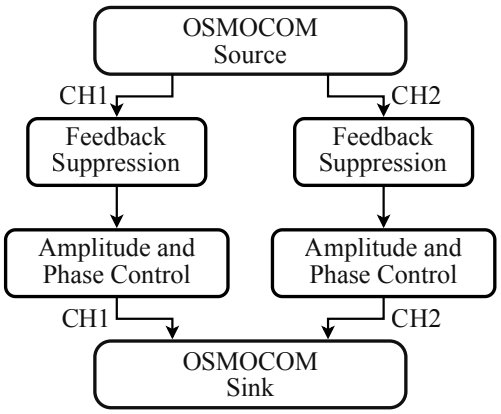

Fig. 5. Flow diagram of the GNU Radio processing.

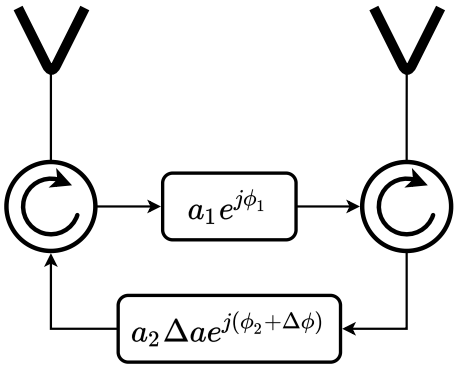

Fig. 6. Jammer paths with calibration adjustments.

C. Cross-eye Jammer

GNU Radio version 3.8 was used to connect the two receive and transmit channels internally in a repeater configuration, while also applying amplitude and phase control to both paths. A summary of the flow diagram of the GNU Radio software implementation can be seen in Fig. 5.

Two OsmoSDR blocks were used to interface with the SDR. A GNU Radio Companion flowgraph was used to control the amplitude and phase of each path, and the gain of each channel in real-time. The amplitude control was applied by multiplying the path by the set value, while phase control was applied by multiplying the path by $e^{j\psi}$, where ψ was the set phase value.

One particularly challenging aspect of retrodirective cross-eye jamming implementation is achieving sufficient isolation between the two repeaters comprising the jammer to avoid spurious echoes and oscillation [2], [5]. For this system, a four-fold solution was applied. Firstly, the power dividers with high isolation were used, as stated above. Then, due to the short range of operation, low gains could be used by the jammer repeaters to mitigate feedback without compromising the signal-to-noise ratio (SNR). Finally, a two-stage feedback reduction algorithm was implemented in GNU Radio.

This algorithm worked by nulling the received signal when the magnitude was higher than a specified threshold as such high signals could only be caused by a transmission from the jammer. In addition, the received signal was also nulled when it was below a certain threshold to prevent the transmission of a noise-only signal.

Any spurious signals that arose despite these measures would not adversely affect the results as the large latency of the jammer would prevent interference with the repeated jammer signal. This large latency is a result of the signals having to travel between the computer and the SDR via Universal Serial Bus (USB), and having to be processed by a normal computer system, neither of which is optmised for low latency.

D. Jammer Path Calibration

A high cross-eye gain is only achieved if the jammer parameters are extremely close to their ideal values [5], [13]. As a result, calibration of the relative amplitude and phase of the two jammer channels is an important pre-requisite to cross-eye jammer measurements.

The unknown magnitudes of the two jammer paths are denoted a_1 and a_2, while the unknown phases are denoted ϕ_1 and ϕ_2 in Fig. 6. The relative amplitude and phase of the two jammer channels can be calibrated by varying one of the channels, as shown in Fig. 6, where the calibration magnitude and phase being denoted Δa and $\Delta\phi$, respectively.

Calibration was based on the observation that the sum-channel return from a cross-eye jammer is small as the two signals from the jammer cancel. As the monopulse radar used to test the jammer was available, it could be used to monitor the sum-channel return as the jammer parameters were varied. While this would clearly not be possible in an operational system, it is believed to be reasonable for laboratory experiments.

Calibration started with pointing the radar boresight towards the centre of the jammer and rotating the jammer so that it was broadside on to the radar. Antenna patterns vary the least near the centres of their main beams, so these rotations minimised the influence of the antenna patterns on the calibration.

Both channels of the radar were then enabled, and the radar sum-channel return monitored. The relative phase of the two channels, $\Delta\phi$, was then varied until the minimum sum-channel return was obtained. The benefit of varying the phase first is that a phase difference of 180° will always give the lowest sum-channel return, while the same is not true for a relative amplitude of

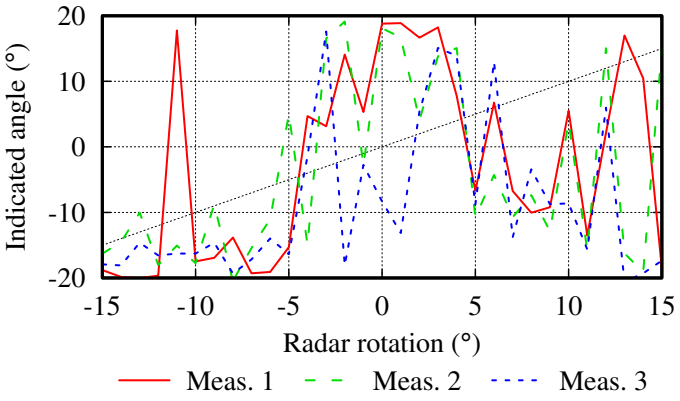

Fig. 7. Three measurements of the indicated angle after jammer calibration.

1. Once the relative phase was optimised, the relative amplitude, Δa was varied until the sum-channel return again reached its minimum. At this point, the two paths through the jammer should have equal amplitudes and a phase difference of 180°. Uncertainty about exactly when the sum-channel minimum is obtained may arise due to noise, and in such cases, it may be necessary to repeat this procedure. However, such repetitions were not required for the measurements described below.

The success of this jammer calibration scheme is seen in Fig. 7, where large indicated angles are measured for a calibrated jammer system. The sum-channel return from the jammer has been calibrated to be so small that the sum-channel return is dominated by noise, which leads to the large variations seen in Fig. 7. Despite the large variations, the large indicated-angle values in Fig. 7 demonstrate that a high cross-eye gain, G_C, has been achieved.

While a high cross-eye gain is desirable, the large variations seen in Fig. 7 will make comparisons to theory extremely challenging as the sum-channel return cannot be accurately determined. As a result, the relative phase of the jammer channels, ϕ, was changed by 5° for the measurements below to give a cross-eye gain, G_C, which is small enough to provide a measurable sum-channel return, but still large enough to create a large angular error.

IV. Measurement Compensation

The idealised configuration of a cross-eye jammer shown in Fig. 2, where the radar and jammer rotate around their centres, is extremely difficult to obtain in practice as a result of considerations such as available mounting brackets. More realistic scenarios are shown in Fig. 8, where the radar and jammer rotate around points offset from their centres. Additionally, there will

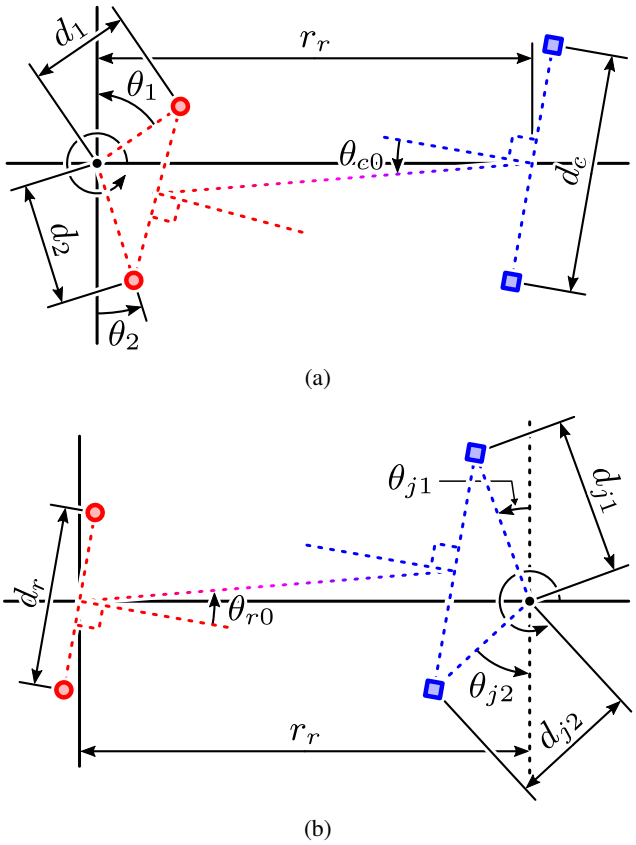

Fig. 8. Configurations when the (a) radar and (b) jammer are rotated, showing the geometrical parameters used in the compensation model.

be amplitude and phase differences between the radar channels that need to be compensated for. Finally, the physical layout of the anechoic chamber and the limited capabilities of the equipment available meant that it was not possible to accurately measure the system configuration. The combined effect of these factors is seen in Fig. 9, where it is seen that the indicated angle is not equal to the radar rotation, and the positions of the jammer antennas converge as the radar rotation angle increases. The measured data must thus be processed to determine the values of the geometric parameters in Fig. 2 and the jammer amplitude and phase differences (a and ϕ, respectively) to allow comparisons to theoretical results to be made.

The geometrical parameters introduced in Fig. 8 account for the cases where the radar and jammer antennas are rotated around a point other than their centres. When the radar is rotated as shown in Fig. 8(a), d_1 and d_2 are the distances from the rotation centre to the antennas, and θ_1 and θ_2 determine the angular positions of the antennas. When the jammer is rotated, d_{j1}, d_{j2}, θ_{j1}, and θ_{j2} fulfil the same roles as d_1, d_2, θ_1, and θ_2 for the radar, respectively, as shown in Fig. 8(b). The remaining

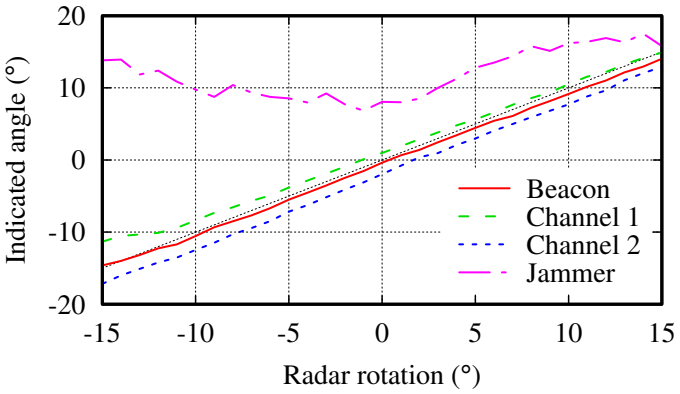

Fig. 9. Plots of the mean indicated angle from five measurements prior to measurement compensation.

new geometrical parameters in Fig. 8 are the distance between the rotation centres, r_r, and the rotation of the stationary system, θ_{r0} and θ_{c0} for the radar and jammer, respectively.

The two channels of the radar receiver will have slight amplitude and phase differences on boresight, and these values are accounted for by model parameters a_r and ϕ_r, which are the amplitude and phase of one of the channels relative to the other.

The final parameters required are those required to characterise the jammer system. As shown in (7), the nature of a cross-eye jammer is such that the jammer parameters only influence the result through the cross-eye gain, G_C, making it impossible to uniquely determine the individual jammer parameters a and ϕ. As a result, only the cross-eye gain is required to characterise the engagement.

Once these system parameters were known, it was possible to determine the corresponding parameters of the mathematical models summarised by Fig. 2, (2), (5), (6), and either (4) or (7) to (9) for the traditional or extended analyses, respectively. These parameters were then used to compensate the measurements for non-idealities not present in the theoretical models, allowing the measured and theoretical results to be compared.

The values of the model parameters were adjusted to give the best possible agreement between the measurements and the mathematical model in (6). This was done using the sequential quadratic programming (SQP) algorithm in GNU Octave version 6.2.0 to minimise the magnitude of the difference between the indicated angles from the measurements and the model. Throughout this process, care was taken to ensure that the parameter values obtained agreed with those noted during the measurements.

Four different measurements were used to fit each set of parameters. The first of these measurements was a beacon case with a target positioned at the centre of the jammer to allow the radar parameters to be determined. The second and third measurements were of the jammer with only one of its two paths active (i.e. $a = 0$ or $a \to \infty$) as these measurements will allow the geometry of the jammer to be determined. Finally, a measurement with the cross-eye jammer operating as a cross-eye jammer was performed both to determine the cross-eye gain, G_C, and to generate the results that are the goal of this work.

TABLE I
SYSTEM PARAMETERS

Parameter	Radar rotated	Jammer rotated
Jammer amplitude difference (a)	−0.2031 dB	−2.731 dB
Jammer phase difference (ϕ)	176.4°	176.8°
Cross-eye gain (G_C)	10.34	6.219
Radar antenna separation (d_r)	0.1266 m	
Range (r)	8.000 m	
Jammer antenna separation (d_c)	0.4049 m	1.217 m

V. RESULTS AND DISCUSSION

The main parameters of the systems used for the two sets of measurements (radar rotated and jammer rotated) are summarised in Table I. Both sets of measurements used high cross-eye gain and large separations of the jammer antennas as required to obtain large angular errors.

A. Radar Rotation

The compensated results for five measurements of the case where the radar was rotated are given in Fig. 10.

Fig. 10(a) shows the results obtained when the jammer system was configured to act as a simple Van-Atta beacon, and as expected, the indicated angle is equal to the radar rotation. Fig. 10(b) shows the radar results for the individual jammer paths, when the other path was disabled. These results demonstrate that the monopulse radar operated correctly, making the radar a suitable platform to test the cross-eye jammer against.

The compensated results are shown in Fig. 10(c). It can be seen that large angular errors were induced in the radar, and that these errors were highly non-linear. The indicated angle of the radar was also never near 0°,

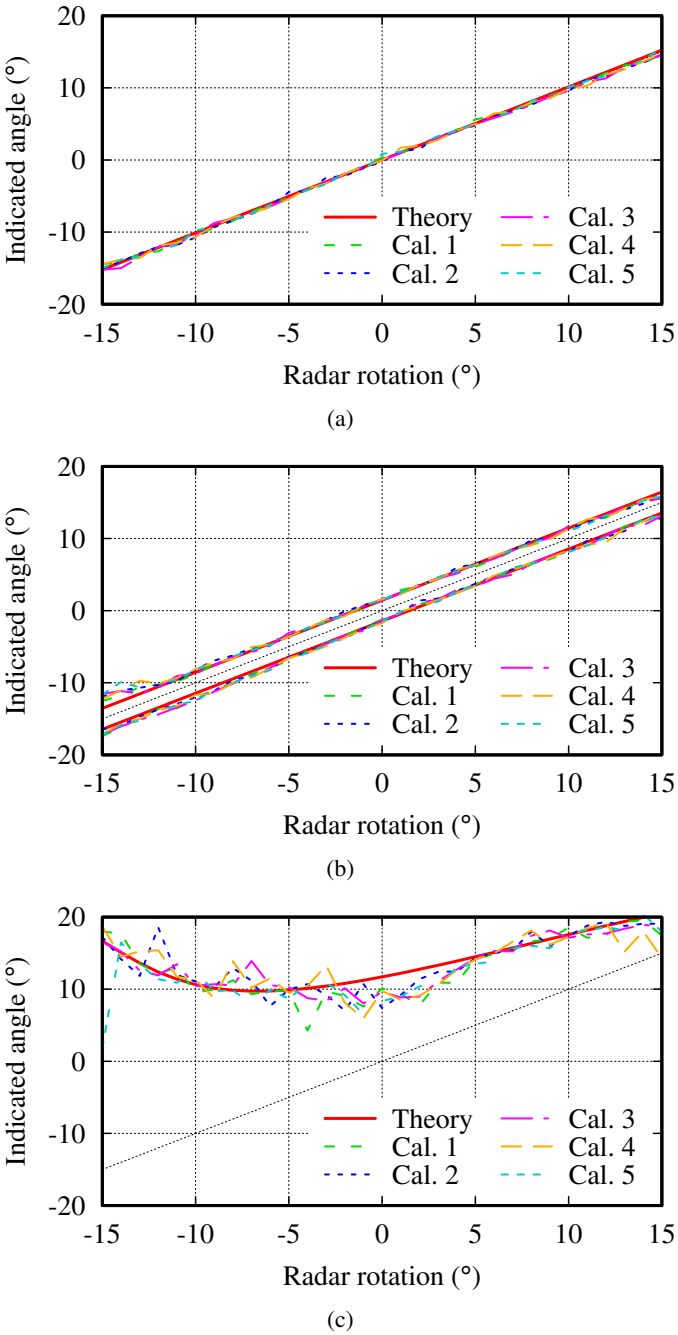

Fig. 10. The compensated indicated-angle measurements for the (a) beacon, (b) isolated jammer channels, and (c) jammer. Some of the individual plots are difficult to discern as they are almost identical.

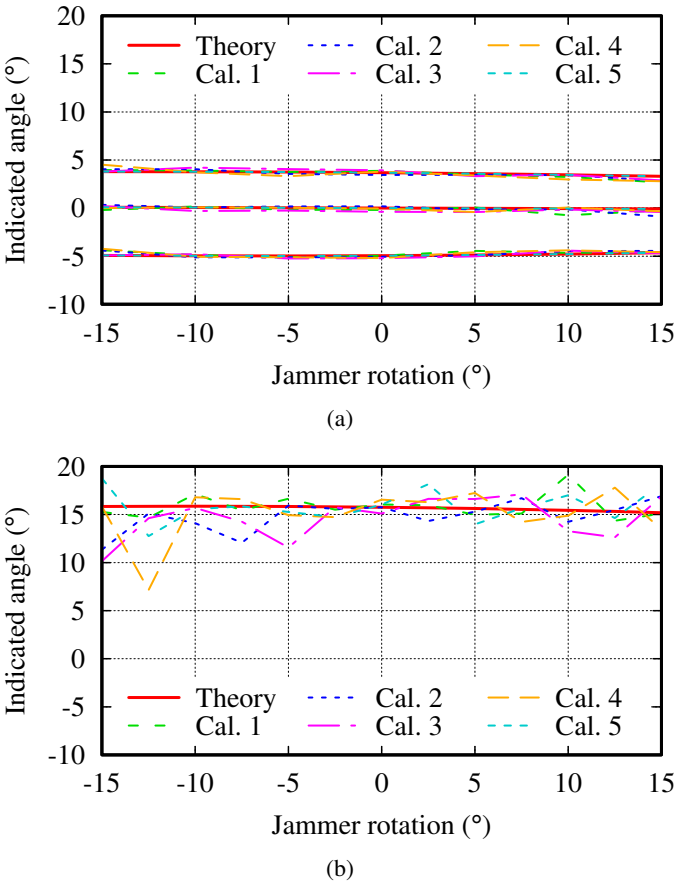

Fig. 11. The compensated indicated-angle measurements for (a) the beacon (the centre results around 0°) and isolated jammer channels (the upper and lower results), and (b) the jammer. Some of the individual plots are difficult to discern as they are almost identical.

suggesting that a tracking radar could lose its lock on a target. These results agree well with the predictions of the extended analysis, and the theoretical curve in Fig. 10(c) is a good match to the measured results, thereby validating the extended analysis.

The small differences between the measured and theoretical curves from roughly $-5°$ to $5°$ in Fig. 10(c), are believed to be a result of non-idealities that are not considered by the theoretical analysis, potentially including factors such as coupling between the radar antennas and squinting of the radar and/or jammer antennas. It is also possible that portions of the measurement system (e.g. the edges of the tapered portion of the anechoic chamber) may have had small effects on the results. The effects of such non-idealities are small, but the nature of cross-eye jamming is that small differences between large signals can be significant, especially in the sum channel.

B. Jammer Rotation

The results obtained from five measurements when the jammer was rotated are given in Fig. 11.

The indicated angles for multiple jammer rotations when the system is configured to act as a beacon are the centre curves around 0° in Fig. 11(a). It can be seen that very little deviation of the indicated angle from the radar boresight was present. This result proves that a

retrodirective beacon was implemented as the position of the beacon does not depend on its rotation.

The indicated angles of the isolated jammer paths are shown as the upper and lower curves in Fig. 11(a) for multiple jammer rotations. It can be seen that the indicated angle to the transmitting antenna for both channels displayed very little deviation from the theoretical results. The positions of the jammer antennas move very slightly towards the centre of the jammer (0° as noted above) as a result of the way the angular separation of the jammer antennas as seen by the radar, θ_e, decreases as the jammer rotates away from broadside on (θ_c changes from 0°). It is also noteworthy that the jammer antennas are not symmetrically positioned around the beacon direction, and this is a result of the large amplitude difference between the two channels (−2.731 dB from Table I) causing the beacon position to be closer to the antenna with the higher amplitude.

Fig. 11(b) shows the indicated angle of a cross-eye jammer as the jammer was rotated. It can be seen that a fairly constant angular error of more than 15° was obtained for all rotations, showing that the orientation of the jammer does not affect its performance, proving that the system was retrodirective. The small variation that is seen is again due to the effective spacing between the jammer antennas, θ_e, reducing as the jammer rotates.

VI. Conclusion

The results obtained when a retrodirective cross-eye jammer was tested against a monopulse radar were presented. The system configuration was described with details of the hardware and software systems being provided. A procedure to calibrate a cross-eye jammer was outlined and was shown to lead to high cross-eye gain values. A compensation model and procedure that allow comparisons to theoretical results to be made by compensating for the fact that the radar and jammer were not rotated their centres was outlined.

The measured results confirmed that the monopulse radar was functioning as expected, making it a suitable basis for testing a cross-eye jammer. The cross-eye jammer system was shown to be retrodirective because the measured indicated angle induced in the radar did not change as the jammer was rotated (the small changes observed were due to the geometry of the system). Finally, the measured results agree well with the extended analysis of cross-eye jamming, especially in terms of response characteristics that are not predicted by the traditional analysis.

References

[1] S. A. Vakin and L. N. Shustov, "Principles of jamming and electronic reconnaissance – Volume I," U.S. Air Force, Tech. Rep. FTD-MT-24-115-69, AD692642, 1969.

[2] L. B. Van Brunt, *Applied ECM*. Dunn Loring, USA: EW Engineering, Inc., 1978, vol. 1.

[3] S. M. Sherman and D. K. Barton, *Monopulse Principles and Techniques*, 2nd ed. Boston, USA: Artech House, 2011.

[4] F. Neri, *Introduction to Electronic Defense Systems*, 3rd ed. Norwood, MA: Artech House, 2018.

[5] W. P. du Plessis, "A comprehensive investigation of retrodirective cross-eye jamming," Ph.D. dissertation, University of Pretoria, Pretoria, RSA, 2010.

[6] W. P. du Plessis, J. W. Odendaal, and J. Joubert, "Extended analysis of retrodirective cross-eye jamming," *IEEE Trans. Antennas Propag.*, vol. 57, no. 9, pp. 2803–2806, Sept. 2009.

[7] J. W. Wright, "Radar glint – a survey," *Electromagnetics*, vol. 4, no. 2, pp. 205–227, Jan. 1984.

[8] L. Falk, C. Arvidsson, S. Berglund, and A. Eneroth, "Simple derivation of crosseye jamming principles," in *MilTech 2 Conf.*, 25-26 Oct. 2005, pp. 93–100.

[9] D. D. Howard, "Radar target angular scintillation in tracking and guidance systems based on echo signal phase front distortion," in *Proc. Nat. Eng. Conf.*, vol. 15, Chicago, USA, 1959, reprinted in Radars, Vol. 4, Radar Resolution & Multipath Effects, David K. Barton, Ed., Artech House, 1975.

[10] J. E. Meade, "Target considerations," in *Guidance*, A. S. Locke, Ed. D. Van Nostrand Co., Inc., 1955, ch. 11, pp. 435–444.

[11] W. P. du Plessis, "Modelling monopulse antenna patterns," in *Saudi Int. Electron. Commun. Photon. Conf. (SIECPC)*, Riyadh, Saudi Arabia, 27-30 Apr. 2013, pp. 1–5.

[12] L. Falk, "Cross-eye jamming of monopulse radar," in *IEEE Waveform Divers. Des. Conf.*, Pisa, Italy, 4-8 Jun. 2007, pp. 209–213.

[13] W. P. du Plessis, J. W. Odendaal, and J. Joubert, "Tolerance analysis of cross-eye jamming systems," *IEEE Trans. Aerosp. Electron. Syst.*, vol. 47, no. 1, pp. 740–745, Jan. 2011.

[14] W. P. du Plessis, "Platform skin return and retrodirective cross-eye jamming," *IEEE Trans. Aerosp. Electron. Syst.*, vol. 48, no. 1, pp. 490–501, Jan. 2012.

[15] W. P. du Plessis, "Limiting apparent target position in skin-return influenced cross-eye jamming," *IEEE*

Trans. Aerosp. Electron. Syst., vol. 49, no. 3, pp. 2097–2101, Jul. 2013.

[16] W. P. du Plessis, "Statistical skin-return results for retrodirective cross-eye jamming," *IEEE Trans. Aerosp. Electron. Syst.*, vol. 55, no. 5, pp. 2581–2591, Oct. 2019.

[17] F. Neri, "Experimental testing on cross-eye jamming," in *AOC Int. Symp. Conf.*, Las Vega, USA, 2000.

[18] W. P. du Plessis, "Practical implications of recent cross-eye jamming research," in *Def. Operational Appl. Symp. (SIGE)*, São José dos Campos, Brazil, 25-28 Sep. 2012, pp. 167–174.

[19] N. M. Harwood, W. N. Dawber, V. A. Kluckers, and G. E. James, "Multiple-element crosseye," *IET Radar Sonar Nav.*, vol. 1, no. 1, pp. 67–73, Feb. 2007.

[20] Y. Jang, J. Park, C. Lee, I. Kim, G. Kim, and S. Cho, "Performance experiment of the angle deception of cross-eye jamming against a monopulse sensor," *J. Electromagn. Eng. Sci.*, vol. 29, no. 2, pp. 146–149, Feb. 2018.

[21] W. P. du Plessis, J. W. Odendaal, and J. Joubert, "Experimental simulation of retrodirective cross-eye jamming," *IEEE Trans. Aerosp. Electron. Syst.*, vol. 47, no. 1, pp. 734–740, Jan. 2011.

[22] F. Pieterse and W. P. du Plessis, "Retrodirective cross-eye jammer implementation using software-defined radio (SDR)," in *IEEE Radar Conf. (RadarConf)*, Atlanta, GA, USA, 7-14 May 2021, pp. 1–4.

[23] L. C. Van Atta, "Electromagnetic reflector," U.S.A. Patent 2 908 002, Oct. 6, 1959.

[24] S. M. Sherman, "Complex indicated angles applied to unresolved radar targets and multipath," *IEEE Trans. Aerosp. Electron. Syst.*, vol. 7, no. 1, pp. 160–170, Jan. 1971.

Frans-Paul Pieterse (S'21, M'21) completed the B.Eng. (Electronic), B.Eng.Hons (Electronic), and M.Eng. (Electronic) degrees from the University of Pretoria in 2017, 2018 and 2022, respectively. He is currently an employee of the Council for Scientific and Industrial Research (CSIR), and his primary research interests are related to radar and electronic warfare (EW).

Warren P. du Plessis (M'00, SM'10) received the B.Eng. (Electronic), M.Eng. (Electronic), and Ph.D. (Engineering) degrees from the University of Pretoria in 1998, 2003, and 2010, respectively, winning numerous academic awards including the prestigious Vice-Chancellor and Principal's Medal. He an Associate Editor of the IEEE Transactions on Aerospace and Electronic Systems.

He spent two years as a lecturer at the University of Pretoria, and then joined Grintek Antennas as a design engineer for almost four years, followed by six years at the Council for Scientific and Industrial Research (CSIR). He is currently a Professor at the University of Pretoria, and his primary research interests are cross-eye jamming and thinned antenna arrays.